Estimation of the total electron content of the Martian ionosphere using radar sounder surface echoes

Ali Safaeinili, Wlodek Kofman, Jeremie Mouginot, Y. Gim, Alain Hérique, Anton Ivanov, Jeffrey Plaut, Giovanni Picardi

Estimation of the total electron content of the Martian ionosphere using radar sounder surface echoes

Ali Safaeinili,[1] Wlodek Kofman,[2] Jérémie Mouginot,[2] Yonggyu Gim,[1] Alain Herique,[2] Anton B. Ivanov,[1] Jeffrey J. Plaut,[1] and Giovanni Picardi[3]

Received 2 October 2007; revised 19 October 2007; accepted 24 October 2007; published 15 December 2007.

[1] The Martian ionosphere's local total electron content (TEC) and the neutral atmosphere scale height can be derived from radar echoes reflected from the surface of the planet. We report the global distribution of the TEC by analyzing more than 750,000 echoes of the Mars Advanced Radar for Subsurface and Ionospheric Sounding (MARSIS). This is the first direct measurement of the TEC of the Martian ionosphere. The technique used in this paper is a novel "transmission-mode" sounding of the ionosphere of Mars in contrast to the Active Ionospheric Sounding experiment (AIS) on MARSIS, which generally operates in the reflection mode. This technique yields a global map of the TEC for the Martian ionosphere. The radar transmits a wideband chirp signal that travels through the ionosphere before and after being reflected from the surface. The received waves are attenuated, delayed and dispersed, depending on the electron density in the column directly below the spacecraft. In the process of correcting the radar signal, we are able to estimate the TEC and its global distribution with an unprecedented resolution of about 0.1 deg in latitude (~5 km footprint). The mapping of the relative geographical variations in the estimated nightside TEC data reveals an intricate web of high electron density regions that correspond to regions where crustal magnetic field lines are connected to the solar wind. Our data demonstrates that these regions are generally but not exclusively associated with areas that have magnetic field lines perpendicular to the surface of Mars. As a result, the global TEC map provides a high-resolution view of where the Martian crustal magnetic field is connected to the solar wind. We also provide an estimate of the neutral atmospheric scale height near the ionospheric peak and observe temporal fluctuations in peak electron density related to solar activity. **Citation:** Safaeinili, A., W. Kofman, J. Mouginot, Y. Gim, A. Herique, A. B. Ivanov, J. J. Plaut, and G. Picardi (2007), Estimation of the total electron content of the Martian ionosphere using radar sounder surface echoes, *Geophys. Res. Lett.*, *34*, L23204, doi:10.1029/2007GL032154.

1. Introduction

[2] MARSIS is a ground-penetrating radar on board the Mars Express (MEX) spacecraft [*Picardi et al.*, 2005]. The primary purpose of MARSIS is to investigate the subsurface of Mars up to a depth of five km to detect buried materials and interfaces, including water ice or liquid deposits. In its first year of operation, MARSIS has mapped the subsurface of the south-polar layered deposits [*Plaut et al.*, 2007] and has identified large radio-transparent areas near the equator associated with volcanic material or possibly ancient ice deposits. Radar waves with frequencies below the plasma frequency of the ionosphere cannot propagate and are either reflected or absorbed. In the subsurface sounding mode, the MARSIS operating band is chosen such that its lowest frequency is above the expected peak plasma frequency. Under this condition, the radar waves reach the surface after being both attenuated and dispersed by the ionosphere. The dispersion is due to the frequency dependence of the radio wave propagation speed in the ionosphere [*Budden*, 1985]. Figure 1a shows the impact of the ionosphere on the radar signal, causing a defocusing and delay of the returned echo that severely compromises interpretability. Unlike attenuation, which causes a reduction in signal to noise ratio and is irreversible, the dispersion (or defocusing) and the delay are generally reversible and are corrected during MARSIS ground data processing, as shown in Figure 1.

[3] MARSIS was designed to operate in the lower HF band (1.3–5.5 MHz) despite the anticipated impact of the ionosphere on radar waves at these frequencies. At low frequencies the wave propagation loss in the subsurface medium is lower that in turn results in a higher penetration depth, balancing against the negative impact of the ionosphere. While the ionosphere creates a problem for the subsurface sounding objectives of MARSIS, it provides a unique opportunity to obtain information about the ionosphere of Mars. By analyzing the MARSIS surface echoes we have been able to derive an accurate estimate for the total electron content of the ionosphere and estimate the scale height of the atmosphere near the ionospheric peak. We have also used the extensive set of data available on the Martian night side (solar zenith angle, SZA > 100 degrees) to establish an apparent correlation between the crustal magnetic field of Mars and regions of high electron concentration in the night side ionosphere.

[4] Mars Global Surveyor's instruments observed the variability of the ionospheric parameters and their correlation with the crustal magnetic field direction [*Krymskii et al.*, 2004]. The authors attributed this correlation to the reconnection between the interplanetary magnetic field and the crustal field and then the penetration of the solar wind particles into the atmosphere. These observations were confirmed by the MARSIS radar operated in the ionosonde mode (AIS experiment) [*Gurnett et al.*, 2005; *Nielsen et al.*, 2007] showing that the AIS signal is reflected by elongated

[1] Jet Propulsion Laboratory, California Institute of Technology, Pasadena, California, USA.
[2] Laboratoire de Planétologie de Grenoble, CNRS, UJF 38041, Grenoble, France.
[3] Infocom Department, "La Sapienza" University of Rome, Rome, Italy.

0094-8276/07/2007GL032154

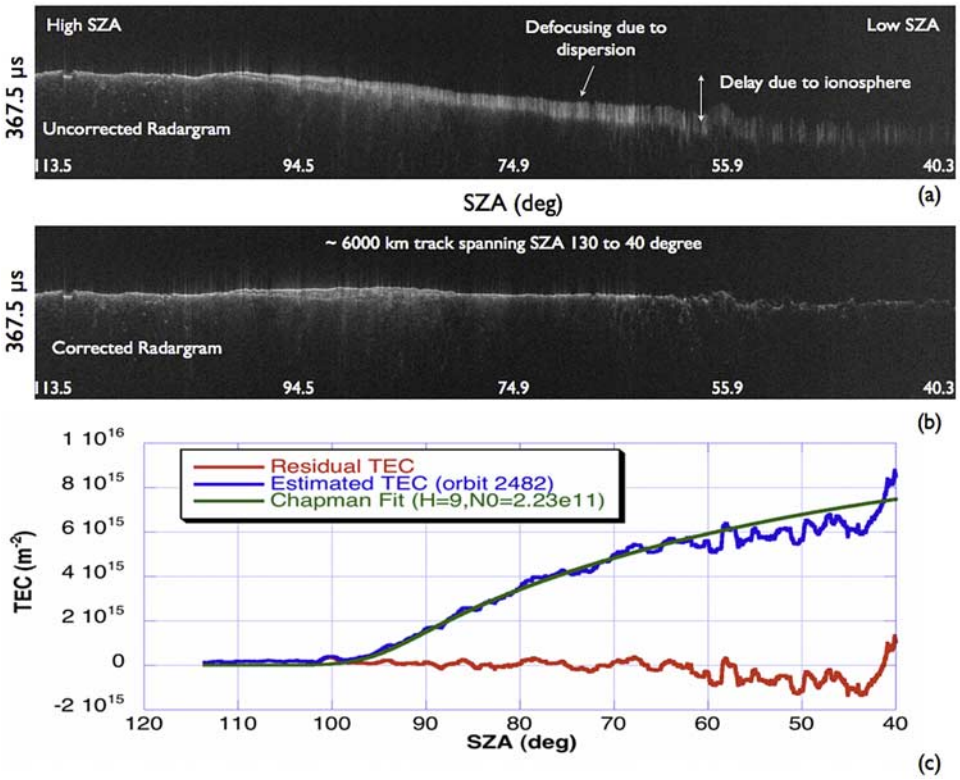

Figure 1. (a) A typical MARSIS radargram without ionospheric phase compensation. The vertical axis is the depth expressed in time, the horizontal axis is the along-track spacecraft position corresponding to sequential measurements and the brightness indicates the amplitude of the signal (white corresponds to larger signal amplitude). This observation starts on the night side (SZA = 115°) and ends on the day side (SZA = 40°) crossing the sunrise terminator. (b) The same radargram after the ionospheric phase correction is applied. The phase correction, which is a function of frequency and SZA, is used to derive the ionospheric parameters. (c) Estimated TEC as a function of SZA for the radargram shown in Figures 1a and 1b. The blue curve shows TEC values independently estimated for each of the 1000 echoes contained in the radargram at ~0.1 degree separation in latitude. The green curve is the best fit TEC model based on the Chapman function. The red curve is the residual TEC obtained by subtracting the best fit Chapman model from the data. The start of this track was at 22:14 and end at 09:47.

structures of the electron density. These structures are localized in the cusp-like regions of the vertical magnetic field. The above conclusions were based on observations of the day side ionosphere. The map presented in this paper extends the observations on the day side to the night side of Mars. Further, the data presented in this article provide a global view of this relationship between the Mars magnetic field and electron concentration that recently has been reported by other workers [*Duru et al.*, 2006; *Nielsen et al.*, 2007]. Our use of ~750,000 independent measurement of the TEC results in a higher confidence in the previously reported relation between the crustal magnetic field and the electron content in the ionosphere on the night side (SZA > 100 degrees). Our findings indicate the presence of small regions that behave like the cusp regions observed on Earth. We believe these regions with higher concentrations of electrons are due to the connection of the solar wind to the Martian night side ionosphere and are likely to occur where the crustal magnetic field component has a large radial component.

[5] Prior to the start of MARSIS data collection, we studied the expected effects of the ionosphere on the sounding signals, and proposed a method to correct them [*Safaeinili et al.*, 2003]. The correction of the radar signal phase is done using an approximate, but sufficiently accurate power expansion of the refractive index of plasma [*Safaeinili et al.*, 2003]. We are able to estimate the total electron content, peak electron density and neutral atmosphere scale height over a relatively narrow 0.1-degree spacing along-track (5 km footprint). The extraction of parameters is possible due to the fact that each MARSIS band covers 1 MHz at roughly 3 kHz resolution steps. The longitudinal resolution depends on the number of orbits available, and it currently is in the order of 2 degrees.

2. Ionospheric Signal Distortion

[6] The MARSIS radar echoes are distorted when traversing the ionosphere resulting in the signal phase changing by an amount $\Delta\varphi$ for each frequency f. This frequency dependent phase distortion causes a defocusing of the signal as shown in Figure 1. The phase distortion can be expressed as

$$\Delta\varphi(f) = -\frac{4\pi f}{c}\int (n(z)-1)dz \qquad (1)$$

$$n(z) = \sqrt{1 - \left(\frac{f_p^2(z)}{f^2}\right)} \approx 1 - \frac{1}{2}\left(\frac{f_p^2(z)}{f^2}\right) - \frac{1}{8}\left(\frac{f_p^2(z)}{f^2}\right)^2 - \frac{1}{16}\left(\frac{f_p^2(z)}{f^2}\right)^3, \quad (2)$$

Where c is the speed of light in free space, n(z) is the refractive index of the ionosphere,

$$f_p(z) = 8.98\sqrt{N_e(z)}, \quad (3)$$

The $f_p(z)$ is a local plasma frequency changing with altitude z. $N_e(z)$ is the electron density profile of the ionosphere traversed by the radar signal. By introducing equations (2) and (3) in equation (1), one obtains the ionospheric phase distortion of the MARSIS radar signal.

$$\Delta\varphi(f) = -\frac{2}{c}\left[\frac{\pi}{f}8.98^2\int N_e(z)dz + \frac{\pi}{3f^3}8.98^4\int N_e^2(z)dz + \frac{\pi}{8f^5}8.98^6\int N_e^3(z)dz\right] \quad (4)$$

Equation (4) indicates how the perturbation of the signal phase depends on the frequency and on the electron density profile. Our analysis has shown that over MARSIS frequency bands, a three-term expansion (equation (4)) is sufficient to correct the signal. The first term is directly proportional to the total electron content, which is the most important parameter characterizing the ionosphere. The second and third terms depend on higher order moments of the electron density profile, providing information about the neutral atmosphere scale height and peak electron density. The influence of each term on the distortion of the signal depends on the frequency, and therefore on the band used by MARSIS. For the highest radar frequency, the second term can reach 10% of the first one, and the third can reach 4% at the central frequency. For the lowest band, the relative importance of the higher order terms is greater and can reach 40%.

[7] Since the coefficients of equation (4) (i.e. the integral terms) are not known a priori, and can vary from echo frame to echo frame, we use an optimization method to find them such that the amplitude of the signal is maximized and the echo delay matches the expected range based on our knowledge of the surface topography using MOLA data [*Zuber et al.*, 1998].

[8] As the phase of the signal depends on the frequency there is a unique solution for these three coefficients. The initial conditions for optimization are calculated using a quadratic model of the density profile close to the maximum height.

[9] The optimization procedure provides the three coefficients shown in equation (4). The first coefficient is directly related to the TEC and has a one-sigma deviation value of $\sim 4 \times 10^{14}$ m^{-2}. The other two depend on the integral of the second and third power of the electron density profile.

[10] Since nearly all of the MARSIS signal distortion is due to the electron content at altitudes under 200 km, we choose to approximate the electron density profiles for SZA less then 100 degrees by Chapman's model [*Chapman*, 1931]. Chapman expressed the electron density profile of the ionosphere as

$$N_e(z) = N_0 \exp\left[0.5\left(1 - \frac{z - z_0}{H} - Ch\left(\frac{R_m + z_0}{H}, \chi\right) \cdot \exp\left(-\frac{z - z_0}{H}\right)\right)\right] \quad (5)$$

where z_0 is the height of the peak for the electron density profile for SZA = 0, H is the scale height of the atmosphere, R_m is the radius of Mars, χ is the solar zenith, and N_0 is the maximum electron density of the ionosphere at $\chi = 0$. *Ch*() is the Chapman *grazing* function [*Chapman*, 1931]. As shown previously by other workers [see *Withers and Mendillo*, 2005, and references therein] the main peak of electron density profile is situated at altitudes of about 130–150 km during the day and the profile is consistent with the one described by the Chapman model. Although approximate, the use of the Chapman function with a constant parameter enables us to condense the ionospheric profile information into two key parameters, N0 and H. It is then possible to study the average behavior of the ionospheric profiles by tracking the N0 and H parameters. It is understood that N0 and H represent the average parameters close to the electron density maximum and may not accurately represent the actual peak electron density or neutral scale height for all profiles.

[11] To obtain N0 and H, we fit curves for the first three moments of the electron density profile shown in equation (4). These moments are estimated for a range of SZA in a given orbit and are used to constrain the N0 and H estimation. The expected TEC curve is derived from the Chapman profile using obtained N0 and H and shown in Figure 1c.

3. Ensemble TEC Data

[12] Figure 1c shows the derived values of the TEC as a function of SZA for the radargram shown in Figure 1 and displays the typical behavior of the TEC. It demonstrates the rapid variation of the TEC as a function of spacecraft along-track position, which indicates significant inhomogeneity in the ionosphere of Mars. Both N_0 and H are varied to obtain the best fit (method explained above) to the Chapman model as shown in Figure 1c. As shown in Figure 1c, a Chapman function TEC versus SZA curve fits the overall shape of the estimated TEC curve well for SZA less than 100. This good fit indicates that the ionosphere below 200 km behaves like the terrestrial E region, where the production of ionization is balanced by recombination, proportional to the square of the electron density. Every MARSIS orbit yields a single value for the peak electron density N_0 and the atmospheric scale height H from the estimated phase corrected coefficients values as a function of SZA.

[13] We analyzed a set of ~750 orbits spanning the observations from June 2005 to September 2006. These orbits cover SZA of 45° to 130° and a range of sun-Mars distances from perihelion to aphelion and the F10.7 index varied on average from 90 in the beginning of this period to 80 (10^{-22} W * m^{-2} * Hz^{-1}) at the end of this period.

[14] Figure 2 shows the distribution of peak electron density N_0 and scale height H for all available data in the

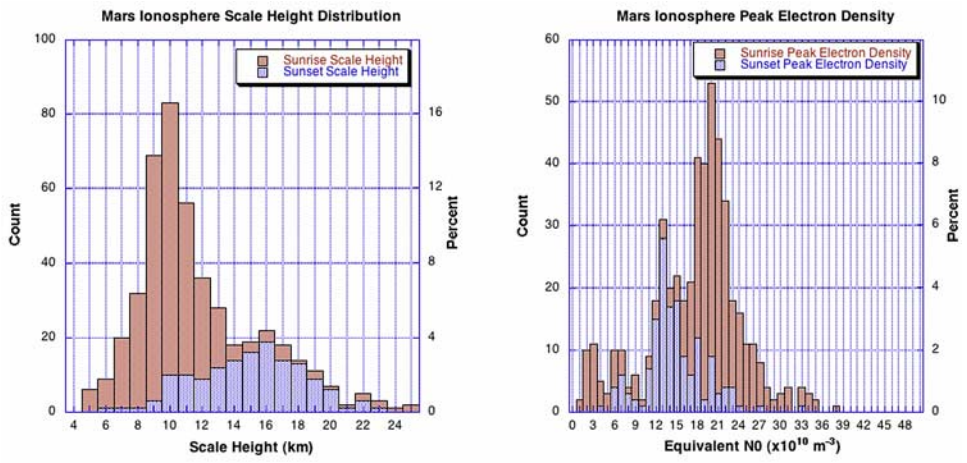

Figure 2. Histograms of the Chapman model parameters N_0 and H. (left) The histogram of the scale height H. The sunset group is highlighted in blue clearly indicating the second mode of the distribution. (right) The extrapolated N_0 value based on the Chapman fit.

period of interest mentioned above. The range of SZA used for the derivation of the ionospheric parameters is between 60° to 100°, which corresponds to the condition where we have good surface echoes enabling a reliable estimation of ionospheric parameters using a Chapman function model. The mean value for the scale height is 11.5 km, with a variance of 3.5 km and for the N_0 2.1 $\times$ 10^{11} m^{-3} with a variance of 0.6 $\times$ 10^{11} m^{-3}. This is the first time that these parameters are measured in the topside mode where the entire electron column between the spacecraft and the ground are measured and are based on more than 500 Chapman profiles. Both distributions are bi-modal, which seems to be related to the local time of the observations. Separating the data by the local time of the terminator crossing, i.e. whether the pass included the sunset or sunrise terminator we get two distinct populations. The sunrise orbits tend to have a smaller scale height of 10 km, and the sunset orbits have a scale height of 15 km. Similarly, the equivalent extrapolated N_0 is higher for sunrise orbits at $\sim$2.1 $\times$ 10^{11} m^{-3} and is lower for the sunset orbits at about 1.3 $\times$ 10^{11} m^{-3}. The sunset and sunrise parameters can be considered as bracketing the range of actual values during the diurnal cycle.

4. Global Electron Distribution

[15] By combining all of our data in the selected period, we generated a global view of the electron distribution in the Martian night side ionosphere. In Figure 3a, bright regions correspond to locations with electron content higher than average value calculated for the night time portion of that orbit (SZA > 100 degree). Figure 3b shows the magnitude of the vertical component of the magnetic field Br. The magnetic field shown is based on a crustal magnetic field model [*Langlais et al.*, 2004] using the Mars Global Surveyor magnetometer instrument data [*Connerney et al.*, 2001]. Figure 3c shows an example of the connection between the TEC and the direction of the magnetic field over a single track. Since the quantities are not linearly related, in order to measure the correlation, we apply the Spearman Rank correlation [*Spearman*, 1904] and obtain a value of 0.9. Our results indicate higher concentration of electrons in regions where the magnetic field is vertical and strong enough to be detected by the MGS magnetometer. However, there are areas where a higher concentration of electrons is observed while no vertical magnetic field is indicated by the model or vice versa. This may be explained by a more complex mechanism where factors other than magnetic field normal component control the process. Our observation is consistent with other observations based on radio occultation data [*Krymskii et al.*, 2004] and MARSIS AIS [*Gurnett et al.*, 2005; *Duru et al.*, 2006]. For the first time, we have an adequate coverage of the night side ionosphere to show a more complete picture of the connection between the magnetic field and localized concentration of electrons in the night side ionosphere. The draping of the solar wind around the planet presumably allows the connection between the interplanetary and the Martian crustal magnetic fields. This mechanism was proposed by *Acuña et al.* [1998] and more recently, *Nagy et al.* [2004], *Krymskii et al.* [2004], and *Duru et al.* [2006]. This connection between the solar wind plasma and the atmosphere can result in ionizing of the atmosphere and in the heating of the ionospheric electrons that in turn, slow the recombination process and produce a higher free electron content.

5. Conclusions

[16] The analysis of MARSIS surface echoes has provided high-resolution TEC profiles, neutral atmosphere scale height close to the electron density peak, peak electron density and a picture of the intricate global connection between the crustal magnetic field and the ionosphere of Mars. These data provide a global map of the electron distribution in the ionosphere at night revealing a close connection between the crustal magnetic fields and the solar wind on a global scale. It shows a correlation between the vertical crustal magnetic field and the increase in the total electron content in the night sector of the ionosphere. Over the next 4 years, the Mars Express spacecraft is expected to significantly improve its night time coverage due to the spacecraft orbital evolution in which the periapsis passes will drift further into the night. As MARSIS improves its

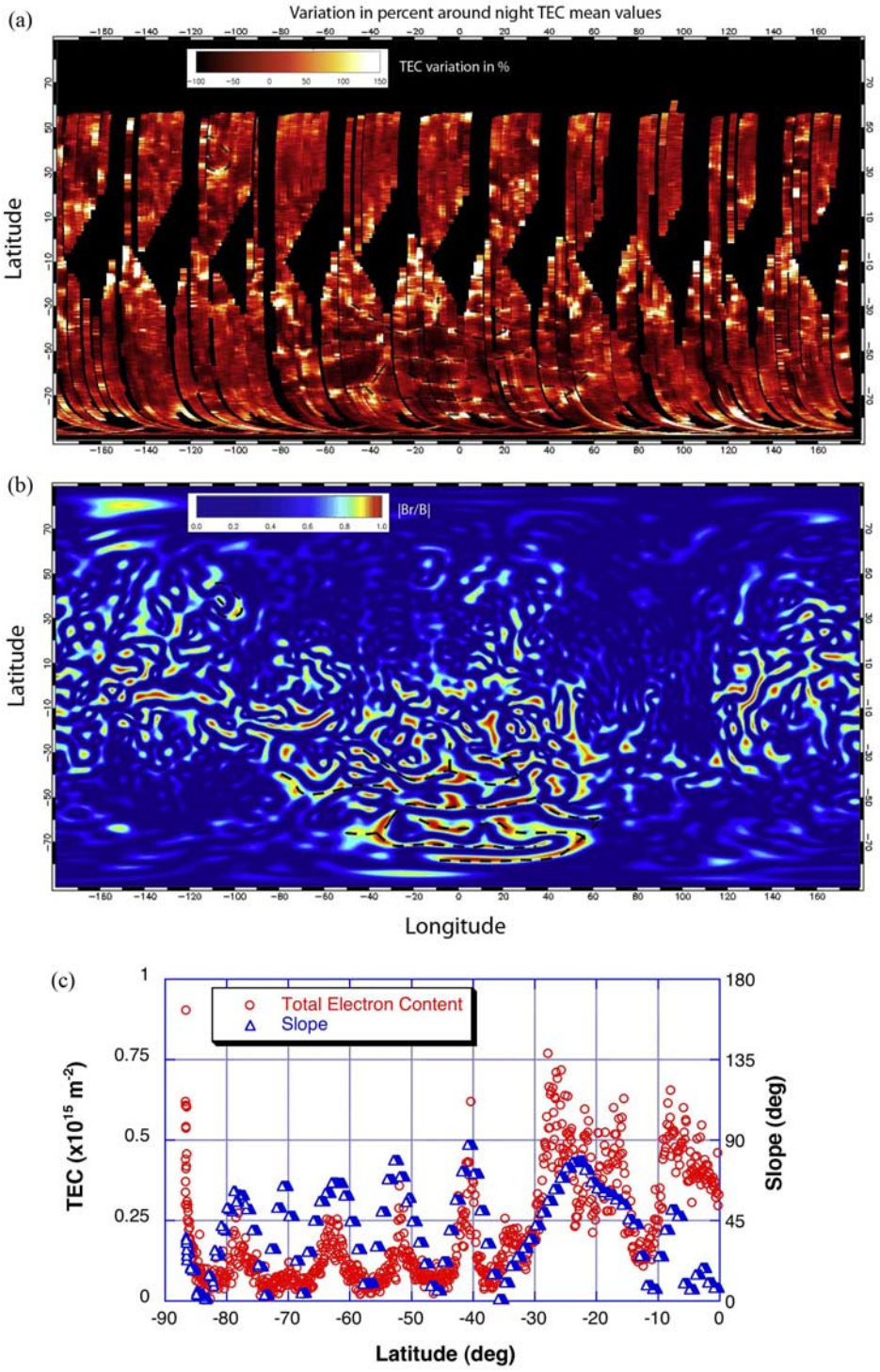

Figure 3. Analysis of MARSIS surface echoes yields a map of total electron content of the ionosphere of Mars. (a) The relative electron distribution map in the night side (SZA > 100). The yellow-colored areas correspond to regions where the TEC is above average in the night side, while the red-colored regions correspond to areas with lower than average TEC. (b) A magnetic map of Mars, derived from a model provided by *Langlais et al.* [2004], where bright areas are regions where the magnetic field is vertical. The dotted lines correspond to the regions where correlation is clearly seen. We propose that these areas are more likely to have higher than average electron content in the night time due to their connection to the solar wind. (c) The TEC (circle) and magnetic field slope (triangle) are shown versus latitude for a MARSIS track at ∼167 east longitude. The plot indicates an enhancement in the TEC over regions where the magnetic field is vertical.

coverage, especially during the night side, we will be able to provide an even more precise map of the regions where the solar wind connects to the crustal magnetic field.

[17] **Acknowledgments.** The authors acknowledge the support of the space agencies of Italy (ASI) and the United States (NASA), for the development and science operations of MARSIS. Operations of the Mars Express spacecraft by the European Space Agency are gratefully acknowledged. Some of the research described in this publication was carried out at the Jet Propulsion Laboratory, California Institute of Technology, under a contract with NASA. The French space agency (CNES) supports these studies in LPG. The authors would like to dedicate this work to our colleague and dear friend Tor Hagfors.

References

Acuña, M. H., et al. (1998), Magnetic field and plasma observations at Mars: Initial results of the Mars Global Surveyor mission, *Science*, *279*(5357), 1676–1680, doi:10.1126/science.279.5357.1676.

Budden, K. G. (1985), *The Propagation of Radio Waves*, Cambridge Univ. Press, New York.

Chapman, S. (1931), Absorption and dissociative or ionising effects of monochromatic radiation in an atmosphere on a rotating earth, *Proc. Phys. Soc. London*, *43*, 1047–1055.

Connerney, J. E. P., M. H. Acuña, P. J. Wasilewski, G. Kletetschka, N. F. Ness, H. Rème, R. P. Lin, and D. L. Mitchell (2001), The global magnetic field of Mars and implications for crustal evolution, *Geophys. Res. Lett.*, *28*(21), 4015–4018, doi:10.1029/2001GL013619.

Duru, F., D. A. Gurnett, T. F. Averkamp, D. L. Kirchner, R. L. Huff, A. M. Persoon, J. J. Plaut, and G. Picardi (2006), Magnetically controlled structures in the ionosphere of Mars, *J. Geophys. Res.*, *111*, A12204, doi:10.1029/2006JA011975.

Gurnett, D., et al. (2005), Radar soundings of the ionosphere of Mars, *Science*, *310*(5756), 1929–1933, doi:10.1126/science.1121868.

Krymskii, A. M., N. F. Ness, D. H. Crider, T. K. Breus, M. H. Acuña, and D. P. Hinson (2004), Solar wind interaction with the ionosphere/atmosphere and crustal magnetic fields at Mars: Mars Global Surveyor Magnetometer/Electron Reflectometer, radio science, and accelerometer data, *J. Geophys. Res.*, *109*, A11306, doi:10.1029/2004JA010420.

Langlais, B., M. E. Purucker, and M. Mandea (2004), Crustal magnetic field of Mars, *J. Geophys. Res.*, *109*, E02008, doi:10.1029/2003JE002048.

Nagy, A. F., et al. (2004), The plasma environment of Mars, *Space Sci. Rev.*, *111*, 33–114, doi:10.1023/B:SPAC.0000032718.47512.92.

Nielsen, E., X.-D. Wang, D. A. Gurnett, D. L. Kirchner, R. Huff, R. Orosei, A. Safaeinili, J. J. Plaut, and G. Picardi (2007), Vertical sheets of dense plasma in the topside Martian ionosphere, *J. Geophys. Res.*, *112*, E02003, doi:10.1029/2006JE002723.

Picardi, G., et al. (2005), Radar soundings of the subsurface of Mars, *Science*, *310*(5756), 1925–1928, doi:10.1126/science.1122165.

Plaut, J. J., et al. (2007), Subsurface radar sounding of the south polar layered deposits of Mars, *Science*, *316*(5821), 92–95, doi:10.1126/science.1139672.

Safaeinili, A., W. Kofman, J.-F. Nouvel, A. Herique, and R. L. Jordan (2003), Impact of Mars ionosphere on orbital radar sounder operation and data processing, *Planet. Space Sci.*, *51*, 505–515, doi:10.1016/S0032-0633(03)00048-5.

Spearman, C. (1904), The proof and measurement of association between two things, *Am. J. Psychol.*, *15*, 72–101.

Withers, P., and M. Mendillo (2005), Response of peak electron density in martian ionosphere to day-to-day changes in solar flux due to solar rotation, *Planet. Space Sci.*, *53*, 1401–1418, doi:10.1016/j.pss.2005.07.010.

Zuber, M. T., et al. (1998), Observations of the north polar region of Mars from the Mars Orbiter Laser Altimeter, *Science*, *282*(5396), 2053–2060, doi:10.1126/science.282.5396.2053.

Y. Gim, A. B. Ivanov, J. J. Plaut, and A. Safaeinili, Jet Propulsion Laboratory, California Institute of Technology, Mail Stop 300-319, 4800 Oak Grove Road, Pasadena, CA 91109, USA. (ali.safaeinili@jpl.nasa.gov)

A. Herique, W. Kofman, and J. Mouginot, Laboratoire de Planétologie de Grenoble, CNRS, UJF 38041, BP 53, F-38041 Grenoble Cedex 9, France.

G. Picardi, Infocom Department, "La Sapienza" University of Rome, Via Eudossiana 18, I-00184 Rome, Italy.